Double resonant Raman phenomena enhanced by van Hove singularities in single-wall carbon nanotubes

J. Kürti,[1] V. Zólyomi,[1] A. Grüneis,[2] and H. Kuzmany[2]
[1]*Department of Biological Physics, Eötvös University Budapest, Pázmány Péter sétány 1/A, H-1117 Budapest, Hungary*
[2]*Institut für Materialphysik, Universität Wien, Strudlhofgasse 4, A-1090 Wien, Austria*
(Received 11 October 2001; revised manuscript received 21 December 2001; published 12 April 2002)

The behavior of the disorder-induced *D* band in the Raman spectrum of single-wall carbon nanotubes (SWCNT's) was investigated both theoretically and experimentally. The measured maximum position of the *D* band for SWCNT bundles exhibits an oscillation superimposed on a linear shift, when the laser excitation energy E_{laser} varies in the range of 1.6–2.8 eV. We have shown theoretically by explicit integrations for the resonant Raman cross section that the *D*-band intensity of an isolated SWCNT has a sharp maximum when E_{laser} of either the incoming or the scattered photon matches a van Hove singularity in the joint density of states. This ''resonance'' must be considered in addition to the double resonance from a scattering by an impurity. Calculating the *D* band of a superposition of all the 114 SWCNT's within a given diameter range, both the shift and the oscillation in the experimentally observed spectra were reproduced.

DOI: 10.1103/PhysRevB.65.165433 PACS number(s): 78.30.Ly, 63.22.+m, 71.20.Tx

I. INTRODUCTION

Single-wall carbon nanotubes (SWCNT's) are targets of intense research in materials science nowadays.[1] Resonance Raman spectroscopy is one of the most powerful tools to obtain useful information about both the electronic and vibronic properties of the tubes.[2] The strongest Raman bands of SWCNT's are the RBM band (radial breathing mode in the range of 100–300 cm^{-1}), and the *G* band [tangential mode(s) at around 1600 cm^{-1}]. Two more, characteristic but weak bands are the *D* band (disorder-induced band in the range of 1300–1400 cm^{-1}) and the G' band at around 2600–2800 cm^{-1}, which is the overtone from *D* band, sometimes also called D^* band. Among these modes the RBM, which is the only one with no counterpart in graphite, proved to be very useful for giving information on the diameter distribution. We have found an oscillatory behavior in the position and the intensity of the RBM band of SWCNT bundles as a function of the laser excitation energy E_{laser}.[3,4] The careful analysis of this oscillation makes it possible to determine the distribution of diameters in such samples.[5] Furthermore, Jorio *et al.* have shown that measuring the RBM band of individual isolated tubes allows the assignment of their (n,m) chirality indices.[6]

Recently, we have found that an oscillation superimposed on a linear shift can be observed also for the position of the *D* and G' bands of SWCNT's.[4,7] A similar anomalous dispersion has also been reported in Refs. 8,9 for the dependence of ω_D and $\omega_{G'}$ on the laser energy E_{laser} in SWCNT's.

To understand the anomalous dispersion of the *D* (and G') bands in SWCNT bundles, a detailed analysis of the similarities to and the differences from the case of graphene (a single sheet of graphite) is needed.

The appearance of the *D* band in the Raman spectrum of disordered graphite has been well known for a long time.[10] The band has its maximum position for visible excitation at around 1350 cm^{-1}, where no peak can be observed in a perfect single crystal of graphite.[10] The intensity of the *D* band increases with increasing disorder. In contrast to the strongest Raman band of graphite (*G* band) at around 1582 cm^{-1}, the position of the *D* band depends on the E_{laser} laser excitation energy.[11–13] The dispersion of the *D* band is nearly linear with a slope of ≈ 50 cm^{-1}/eV, shifting to higher wave numbers with increasing E_{laser}. In addition, there is always a band even for pure, defect-free graphite at about twice the frequency of the *D* band, also showing a dispersion with a slope of about twice the slope of the *D* band. There is some confusion about the nomenclature of the latter band: it is called either D^* band emphasizing that it seems to be the first overtone of the *D* band, or G' band emphasizing that it is an intrinsic feature of the Raman spectrum of graphite that needs no disorder.

The origin of the *D* band in graphite was not understood for several decades. Several approaches were pursued focusing on different aspects of the phenomenon. Either a band-structure picture was used with the introduction of quasi-selection-rules for electrons and phonons[12–14] or the *D* band was treated as a result of a ''breathinglike'' motion of finite clusters.[10,15,16] All suggested descriptions have weak points. The shortcoming of the former approach is that it is based on an *ad hoc* assumption that the wave number of the phonon is the same as the wave number of the excited electron. The latter treatment has its importance for highly amorphous materials, but it is not adequate for describing lightly disordered systems such as the SWCNT's, where a solid-state approximation is more appropriate.

The main problem in the solid-state approximation for graphite with only a small amount of defects lies in the fact that for this material no Γ-point phonons exist in the frequency range between 1300–1400 cm^{-1} at all.[17,18] The only phonons with appropriate frequency are around the *K* point, near the Brillouin zone (BZ) boundary, therefore, these phonons are silent in the usual first-order Raman process. This long-standing problem was solved recently by Thomsen and Reich based on the idea of double resonance.[19] In fact,

Ref. 14 was the first work to state that the double-resonance process is responsible for the dispersion of the *D* band in graphite. However, that paper contains some mistakes, beside the lack of the quantitative treatment of the Raman cross section. According to the description of Thomsen and Reich the incoming photon excites an electron-hole pair and the electron (or hole) is subsequently scattered into another point of the *k* space. After backscattering and a subsequent electron-hole recombination a different photon will be emitted. One of the scattering processes should be mediated by a defect for obtaining the *D* band. The low scattering probability as a consequence of the small concentration of the defects can be compensated by a double resonance, where beside the incoming or outgoing resonance an intermediate state is in resonance as well.

In the present paper, we apply the concepts outlined in Ref. 19 for SWCNT's. We show by explicitly carrying out the integrations of the usual formulas for a resonant Raman process[20] that the most important contributions to the *D* band come from the terms for which not only the double-resonance condition is fulfilled but in addition, the scattering process occurs between electronic states in the *k* space corresponding to van Hove (vH) singularities in the density of states.[21] Summing up the response calculated for the *D* band of more than 100 individual SWCNT's with different diameters and chiralities, we show that the resulting *D* band not only shifts with E_{laser} but there is also an oscillation superimposed on it.[22] The intensity of the *D* band oscillates similarly. We measured the Raman spectrum of a sample of bundles with a given diameter distribution. The calculation for the same diameter distribution reproduces very well the observed anomalous dispersion. An additional conclusion from our calculations is that the position and the intensity of the *D* band are even more sensitive to the diameter distribution than that of the RBM.

The paper is organized as follows. The following section summarizes the basic concepts, and the *D* band of graphene is reviewed with some more qualitative insight into the details; in Sec. III we apply the formalism to individual SWCNT's; in Sec. IV our experimental results are presented and are compared to our calculations of the *D* band for a set of SWCNT's with a Gaussian diameter distribution equivalent to the sample in the experiment; and in Sec. V we summarize our conclusions.

II. BASIC CONCEPTS AND EVALUATION OF THE DOUBLE RESONANCE FOR GRAPHENE

The amplitude of a Raman process can be calculated by perturbation theory and can be visualized by appropriate Feynman diagrams.[20] Figure 1 shows four possible fourth order Feynman diagrams, relevant in our case for a Stokes process. (The anti-Stokes process can be treated similarly.) The vertices 1 and 4 in all four parts of Fig. 1 describe the electron-hole excitation and recombination, respectively. The intermediate vertex labeled by open circles (2 in part I and III, and 3 in part II and IV in Fig. 1) corresponds to a scattering of the electron or the hole by a defect. The remaining vertex in the diagrams corresponds to the creation of a phonon. In principle, similar four diagrams should be taken into account where the first scattering involves a hole instead of an electron. However, such diagrams are equivalent with those shown in Fig. 1 in the case of electron-hole symmetry that is a good approximation at least for the relevant states near the *K* points. We mention that the G' band can be treated similarly, the only difference being that both scattering processes (2 and 3) involve phonons with opposite wave vectors, that is, no defects are needed in that case.

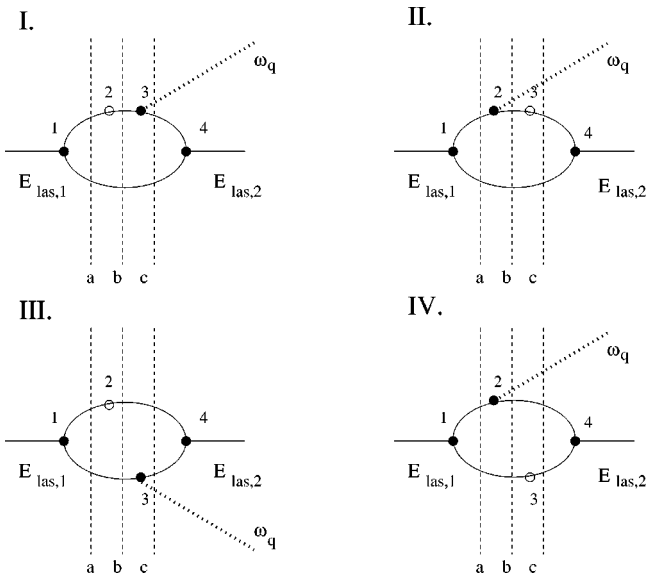

FIG. 1. Fourth-order Feynman diagrams for the Raman process including interaction of the electron or hole with a defect (open circle: 2 in part I, III, and 3 in part II, IV) as well as with a phonon (filled circle: 3 in part I, III, and 2 in part II, IV). The pairs of diagrams (I-III) and (II-IV) differ in the time ordering of the scattering by a defect or a phonon. Only processes where the first scattering involves an electron are shown here. The electron is scattered back in part I and II, whereas in part III and IV the hole is scattered after the electron. Double resonance occurs when the energies of two of the intermediate virtual states (a,b,c) match the laser excitation energy $E_{las,1} \equiv E_{las,2} + \hbar\omega_q$.

The Raman cross section is the absolute square of $K_{2f,10}$, the sum of the complex amplitudes as given by Eqs. (1) and (2) for the various diagrams.[20]

$$K_{2f,10}^{I,III} = \sum_{a,b,c} \frac{M}{(E_{las,1} - E_{el}^{a} - i\gamma)(E_{las,1} - E_{el}^{b} - i\gamma)(E_{las,1} - E_{el}^{c} - \hbar\omega_q - i\gamma)}, \tag{1}$$

$$K_{2f,10}^{II,IV} = \sum_{a,b,c} \frac{M}{(E_{las,1} - E_{el}^{a} - i\gamma)(E_{las,1} - E_{el}^{b} - \hbar\omega_q - i\gamma)(E_{las,1} - E_{el}^{c} - \hbar\omega_q - i\gamma)}. \tag{2}$$

In these formulas 0 and f refer to the initial (ground) and the final states of the material system (graphene), respectively. There is one phonon created, with wave vector $\vec{q}$, in the final state. The total initial and final states contain a photon with $E_{las,1}$ and $E_{las,2}$, respectively. M is a symbolical abbreviation for the transition matrix elements that—together with the damping parameter γ— were assumed to be constant in our calculations, independently of the electronic states.

The ''intermediate'' states (labeled by a, b and c in Fig. 1) may consist of two parts: an electronic and a phononic one (the latter of course only if the phonon already exists: c for all diagrams and also b for diagrams II and IV of Fig. 1). E_{el}^{a}, E_{el}^{b}, and E_{el}^{c} give the electronic part of the energies of the intermediate states. In the case of graphene the treatment of the electronic part is simple: to a good aproximation it is enough to take into account only one electron and one hole state per each K point in the two-dimensional (2D) Brillouin zone. These states are in the π-electron conduction and valence bands, with the one-electron energies of $\varepsilon^{c}(\vec{k})$ and $\varepsilon^{v}(\vec{k})$, respectively. All other states are too far away from the Fermi level and cannot contribute to the resonance with the visible light.

As it is well known, for interaction with visible light, the wave number of the electron and the hole should be practically the same both for the excitation and the recombination processes. The interaction with a phonon, on the other hand, changes the wave number of the electron (or the hole) by $\Delta\vec{k}=\vec{q}$. It follows that for all four diagrams in Fig. 1, $E_{el}^{a}=\varepsilon^{c}(\vec{k})-\varepsilon^{v}(\vec{k})$ and $E_{el}^{b}=\varepsilon^{c}(\vec{k}')-\varepsilon^{v}(\vec{k})$, where $\vec{k}'-\vec{k}=\vec{q}$. E_{el}^{c} is different for the different diagrams: it is $\varepsilon^{c}(\vec{k})-\varepsilon^{v}(\vec{k})\equiv E_{el}^{a}$ in the case of I and II, whereas it is $\varepsilon^{c}(\vec{k}')-\varepsilon^{v}(\vec{k}')$ in the case of III and IV.

The Raman cross section for given initial and final states can be obtained by a summation over all possible intermediate states according to the formulas (1) and (2). For a given phonon wave vector $\vec{q}$, this means an integration over $\vec{k}$ and $\vec{k}'$, with $\vec{k}'-\vec{k}=\vec{q}$. Whereas the energies of the measurable initial ($E_{las,1}$) and final ($E_{las,2}+\hbar\omega_q$) states are equal, the energy conservation does not hold for the intermediate virtual states. The energy denominator depresses the contribution of the intermediate states for which the violation of the energy conservation is large. Resonance occurs on the other hand if an energy denominator is very small. We speak about *double* resonance if the real part of *two* energy denominators become zero at the same time, in at least one term of the sum.[19]

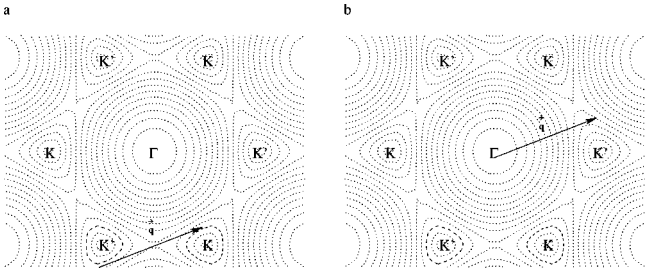

FIG. 2. Schematic equi-excitation-energy (EEE) contours for electrons (a) and equifrequency contours for phonons (b) in 2D graphene. The hexagonal symmetry point (Γ) and the symmetry inequivalent trigonal points (K and K') of the Brillouin zone are indicated in the figure. In the case of double resonance, the wave vector of the phonon $\vec{q}$ connects two K points in the electronic Brillouin zone in the neighborhood of K and K', respectively. Note that only phonons with $\vec{q}$ vectors not too far away from $\vec{q}_0:=\vec{K'K}\equiv\vec{\Gamma K}'$ have the right frequencies needed for the D band.

Figure 2 shows schematically a process that can contribute to double resonance, in the reciprocal space of graphene. The phonon wave vector $\vec{q}$ describes a scattering between two points in the k space of the electrons. Because of the double-resonance condition these two K points have to lay on equi-excitation-energy (EEE) contours with either the same energy or with energies that differ only by $\hbar\omega_q \approx 0.16$ eV. For example, both of these energies are $E_{las,1}$ for incoming resonance in the case of process I in Fig. 1, and $E_{las,2}$ for outgoing resonance in the case of process II of Fig. 1, etc. In all cases this means that both $\vec{k}$ and $\vec{k}'$ should be close to one of the trigonal points (K or K') of the BZ. Furthermore, one has to keep in mind that only phonons with $\vec{q}$ vectors close to $\vec{q}_0:=\vec{K'K}\equiv\vec{\Gamma K}'$ have the right frequencies to contribute to the D band.

For the explicit calculation of the formulas (1) and (2) the usual tight-binding approximation with $t_0=2.9$ eV and neglecting the asymmetries between electron and hole bands was used, which is accepted as a good approximation for the electronic dispersion relation:

$$\varepsilon^{c}(k_x,k_y)=-\varepsilon^{v}(k_x,k_y)=t_0\sqrt{1+4\cos\left(\frac{k_x}{2}\right)\left[\cos\left(\frac{k_x}{2}\right)+\cos\left(\frac{\sqrt{3}k_y}{2}\right)\right]}. \tag{3}$$

The phonon dispersion is not known experimentally around the K (or K') points. Therefore, we used a model dispersion of the same kind as the previous formula, for simplicity:

$$\omega_{ph}(q_x,q_y)=A+B\sqrt{1+4\cos\left(\frac{q_x}{2}\right)\left[\cos\left(\frac{q_x}{2}\right)+\cos\left(\frac{\sqrt{3}q_y}{2}\right)\right]}, \tag{4}$$

where A and B are fitting parameters. We used $A=1200$ cm^{-1} and $B=230$ cm^{-1} based on the experimentally known linear dispersion of the D band of graphite: A was obtained from the extrapolation of the dispersion when the laser excitation energy goes to zero, and B was obtained from the fitting of the slope of the linear dispersion of about 50 cm^{-1}/eV.

Figure 3 shows the results of the integration of the formulas (1) and (2) for graphene, for two different laser excitation

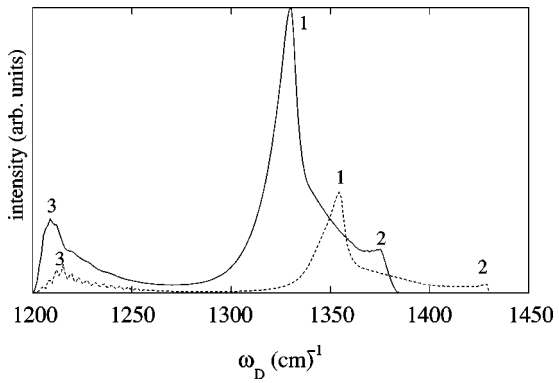

FIG. 3. Calculated *D* band in the Raman spectrum of graphene for $E_{laser}=2.0$ eV (solid line) and $E_{laser}=2.5$ eV (dashed line). The integration for $K^{I}_{2f,10}$ and $K^{II}_{2f,10}$ was carried out using appropriate electron- and phonon-dispersion relations [formulas (3) and (4)].

energies 2.0 eV and 2.5 eV. For the reciprocal lifetime of the electronic states $\gamma=0.03$ eV was used in this case. The spectra consist of several peaks. The origin of these peaks can be understood qualitatively as illustrated in Fig. 4. The main contributions to the *D* band come from the integrations along the two boldface dashed curves that are EEE contours around *K* and K', according to the double resonance. For a given phonon wave-vector transitions between parallel parts of these contours result in local maxima in the integral. The highest intensity occurs for the parts with lowest curvature, labeled by 1 in Figs. 3 and 4. Another local maximum but with lower intensity is obtained for the transitions between the parallel parts with highest curvature, labeled by 2 in Figs. 3 and 4. The difference in the wave vectors for the transitions 1 and 2 depends on the anisotropy (trigonal warping) of both the electron and phonon dispersion relation. For example, if both the electron and the phonon dispersions would be isotropic, the two maxima, 1 and 2 would coincide, because in that case the wave vector for transition 2 is less than q_0 by the same amount by which the wave vector for transition 1 is larger than q_0, and the phonon frequency depends on the absolute value of the deviation of q from q_0. This is the basis

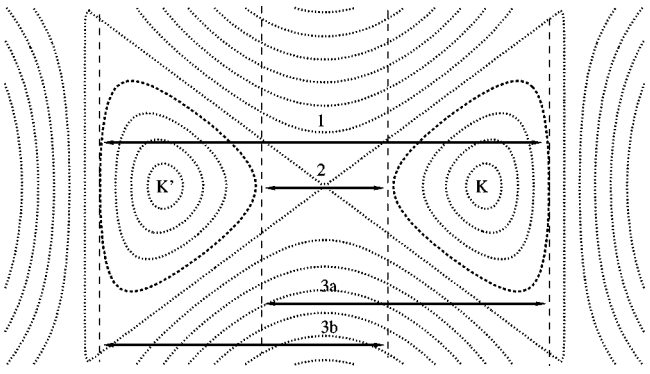

FIG. 4. Simple qualitative interpretation of the maxima 1, 2, and 3 in Fig. 3 (see text). The highest intensity occurs for wave vectors between parallel parts of the EEE contours with lowest curvatures (labeled by 1).

for the $|\vec{q}-\vec{q}_0|=2k$ approximation, where k is the radius of the corresponding EEE contour.[15] This approximation works of course only in the case of isotropic dispersion relations. Furthermore, the wave vectors for the transitions labeled by $3a$ and $3b$ would be exactly q_0 for an isotropic electron dispersion relation, independently from the phonon dispersion. In fact, they are slightly upshifted due to the trigonal warping of the contours. It should be mentioned that the anisotropy is not too large for excitations in the visible, when E_{laser} is in the range of 2–3 eV. All the statements above can be directly verified by comparing the maximum positions of the curves shown in Fig. 3 with the phonon frequencies obtained by the formula (4) using the corresponding wave vectors calculated analytically according to Fig. 4.

The peaks in Fig. 3 shift towards higher wave numbers with increasing laser excitation energy. The reason for this is obvious from Fig. 4. It originates from two facts: First, increasing the laser excitation energy means EEE contours with larger ''radius'' around the *K* and K' points. Second, the transition between the parallel parts of the EEE contours with increasing ''radius'' leads to reduction (2 in Fig. 4) or to an extension (1 in Fig. 4) of the phonon wave vector. The phonon frequency increases in both cases, because the phonon dispersion has a local minimum for $\vec{q}_0$, corresponding to a transition between the *K* and K' points. The upshift of the position of the strongest peak (1) has a slope of 50 cm^{-1}/eV in accordance with the experiments.

The fact that the most important features of the explicit integration can be reproduced by qualitative considerations will be valid also in the case of SWCNT's. This will be very helpful for the interpretation of the anomalous dispersion of bundles of more than 100 different SWCNT's.

III. APPLICATION OF THE THEORY FOR INDIVIDUAL SWCNT'S

The ideas described in the preceding section can be applied to SWCNT's as well. However, there is one essential difference: the 1D nature of the nanotubes results in the vH singularities in the density of states of both the electrons and the phonons. These singularities have an important effect, comparable to the resonance effect due to the zero denominators. As an example, we demonstrate this for the (11,9) nanotube that can be regarded as a typical nanotube in the sample that we measured. Its diameter is very close to the maximum of the diameter distribution obtained from the RBM spectra.[4] Furthermore, it is a chiral nonmetallic tube as most of the tubes in the sample are. However, the conclusions drawn are similar for any other SWCNT.

To evaluate the Raman cross section for the processes shown in Fig. 1, we integrated the formulas (1) and (2) in k space. We used the same tight-binding dispersion relation (3) for electrons as was used for graphene. The only difference is that due to the confinement of the electrons along the circumference of the tube the perpendicular component of the wave vectors is quantized. The wave-vector component parallel to the tube axis remains quasicontinuous. Thus, neglecting the curvature effects, one can use the 2D dispersion re-

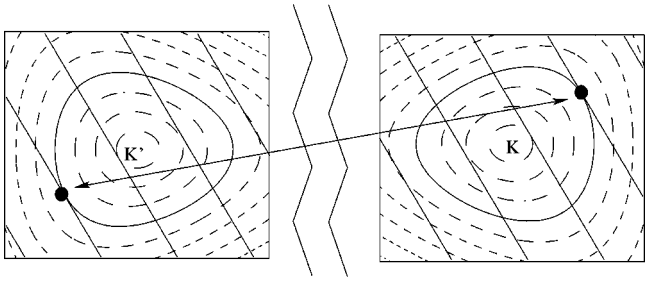

FIG. 5. Dominant transition shown by boldface arrow on the example of a chiral nonmetallic tube (11,9) as plotted in the 2D k space. The zig-zag lines in the center of the figure separate the two ranges of the Brillouin zone around two inequivalent trigonal points (K and K'). The straight lines are the discrete allowed K points for the electrons of the tube. The boldface contours are the EEE contours that touch one of the discrete lines. The positions of the vH singularities in the k space are labeled by filled black circles.

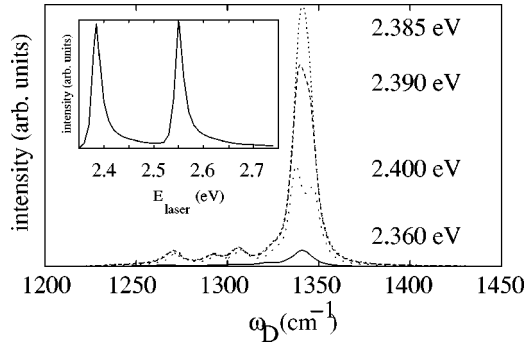

FIG. 6. Calculated D bands by integrating the formulas (1) and (2) for an (11,9) tube in the case of four different laser excitation energies. Note that the third vH singularity in JDOS is at $E_{33}=2.382$ eV. The inset shows the change of the maximum height of the band as a function of E_{laser}. The two maxima in this ''excitation profile'' correspond to the incoming and outgoing resonances.

lation of graphene for SWCNT's but restricting the K points to the allowed parallel straight lines with uniform distances between them. The direction of the lines depends on the chirality angle and the distance between two neighboring lines is $2/d$, where d is the diameter of the tube.[1] Figure 5 shows several discrete lines for the (11,9) chiral tube together with some EEE contours around K and K' points of the BZ. Atmost four of these straight lines can contribute to a resonance process in the visible range. The lines further away from K and K' points do not cross any EEE contours of energies less than 3 eV. Figure 5 shows a situation where an EEE contour touches one of these lines in the neighborhood of both K and K' points. These touching points—labeled by filled black circles in Fig. 5—define the positions of one of the vH singularities in the k space. The corresponding excitation energy is $E_{33}=2.382$ eV for a (11,9) tube using $t_0=2.9$ eV.

Some complications arise concerning the phonon-dispersion relation. According to our experiments, SWCNT bundles have an anomalous dispersion: an oscillation superimposed on the linear upshift (see following section). Although the linear part of the dispersion can be well described by the model formula (4), the oscillating component is more sensitive to the actual phonon-dispersion relation. It turned out that the anisotropy of Eq. (4) is too large and we had to use another model phonon dispersion, where we could tune the amount of the anisotropy (trigonal warping) in order to fit the details of the oscillations quantitatively. The following model dispersion was used:

$$\omega_{ph}(\tilde{q}_r,\tilde{q}_\varphi)=A'+B'\tilde{q}_r[1-\delta\cos(3\tilde{q}_\varphi)], \qquad (5)$$

where $\tilde{q}_r$ and $\tilde{q}_\varphi$ are the polar coordinates of $\vec{\tilde{q}}=\vec{q}-\vec{q}_0$, the deviation of the phonon wave vector from $\bar{\Gamma}\bar{K}'$. $A'=1220$ cm^{-1}, $B'=120$ cm^{-1}, and $\delta=0.06$ proved to be a good combination to describe the measured anomalous dispersion of bundles (see following section). Therefore, the same parameters were used in this section, as well.

The phonon wave vector is determined by the change of the electron wave vector according to momentum conservation ($\vec{q}=\Delta\vec{k}$). We calculated the Raman cross section $|K^I_{2f,10}+K^{II}_{2f,10}+K^{III}_{2f,10}+K^{IV}_{2f,10}|^2$ by integrating along all discrete lines in the neighborhood of the K and K' points, taking into account all possible transitions between them. The results of the integrations can be seen in Fig. 6 for four different laser excitation energies, $E_{laser}=2.360$, 2.385, 2.390, and 2.400 eV, just below and above $E_{33}=2.382$ eV, the third vH singularity in the joint density of states (JDOS). The reciprocal lifetime of the electronic states was $\gamma=0.01$ eV in these calculations. The finite lifetime of the phonons was taken into account by a convolution with a Lorentzian curve with 3-cm^{-1} half width at half maximum.

There are several important conclusions that can be drawn from Fig. 6. First of all, as it is clearly seen in the figure, the D band consist of several subbands, the strongest one being around 1340 cm^{-1}. The origin of the subbands is the following. For an arbitrary E_{laser} that is larger than the second vH singularity in the JDOS ($E_{22}=1.197$ eV) the number of the phonon wave vectors $\vec{q}$ for which the double-resonance condition is fulfilled is at least $4\times4=16$. The actual phonon wave vectors depend on how the discrete lines are cut by the EEE contours in Fig. 5. Even in the case when, due to symmetry reasons, some of the corresponding phonon frequencies are equal, this results in many different D subbands at different positions with different intensities. Some of these subbands may overlap each other. The intensity of the individual components depends on the actual values of the density of states for the electrons in the K points, where the EEE contour cuts the discrete lines. Obviously, at least one vH singularity is involved in the case of the strongest subband at around 1340 cm^{-1}.

The most important conclusion from Fig. 6 is that the intensity of the D band has a sharp maximum when the excitation energy E_{laser} matches a vH singularity. The D band is always determined by the phonons with which the double-resonance condition is fulfilled, but obviously the singularities in the JDOS of the electrons have a comparable effect to this. The explanation for this is straightforward. The strongest possible effect occurs when—besides the double resonance—two vH singularities are matched at the same

time: before as well as after the scattering of an electron (or a hole). This is only possible if the two EEE contours around K and K', for which the double-resonance condition is fulfilled, have the same energy. This can happen only either in process I or III of Fig. 1 in the case of incoming resonance, or in process II or IV of Fig. 1 in the case of outgoing resonance. The inset in Fig. 6 clearly shows the effect of both the incoming and outgoing resonances in the excitation profile for the strongest band at around 1340 cm^{-1}. The ratio of the maximum peak intensity at 2.385 eV to the intensities at 2.35 eV, 2.50 eV, and 2.70 eV are ≈ 39, ≈ 15, and ≈ 20, respectively.

The above conclusions hold for any SWCNT's. This was checked for several tubes with different chiralities. We just mention that the armchair tubes are special in the sense that they have an additional subband at a frequency very close to that corresponding to the K point, with comparable intensity to the other band at higher frequencies. The reason for this is the fact that for armchair tubes there exist always pairs of vH singularities lying on a line that is parallel to the line connecting the points K and K' in the BZ. The wave vector connecting these vH singularities is almost identical to $\vec{q}_0$, in fact it is slightly larger due to the trigonal warping effect.

We summarize the main conclusions of this section as follows. The calculated D band of a SWCNT for an arbitrary excitation energy consist of many subbands, some of them overlapping each other. The positions and intensities of these subbands depend on E_{laser}. The intensity of the D band has a sharp maximum if either the incoming or the outgoing light matches a vH singularity in the JDOS. This behavior can be assigned as a ''triple resonance,'' which is the combined effect of a double resonance plus an enhancement by matching the singularities in the density of states.

IV. COMPARISON OF THE THEORETICAL RESULTS TO THE EXPERIMENTS

A. Experiment

In this section the comparison of the experimental and theoretical results is presented for samples grown by laser ablation at the Rice group. Raman measurements were carried out using 22 different laser excitations in the range between 1.6 eV and 2.8 eV.

The measured intensities were corrected for power of incident laser and for detector sensitivity. The latter was calibrated in a standard way by comparing the response of the F_{2g} line of silicon with reported results.[23]

The diameter distribution was obtained from the analysis of the Raman spectra of the RBM. The oscillation of the position and intensity of the RBM as a function of the laser excitation energy could be described by a Gaussian distribution $w(d) \sim \exp[-(d-d_0)^2/2\sigma^2]$ with a mean tube diameter of $d_0 = 1.32 \pm 0.01$ nm and a distribution width (variance) of $\sigma = 0.14$ nm.[4]

Figure 7 shows the measured D-band spectra. A shift and an oscillation in the position and an oscillation in the intensity of the D band can be clearly seen. Figure 8 shows the dispersion of the maximum position of the D band, extracted from these spectra. For comparison, the behavior of the G band and the G' band are also shown in the figure.

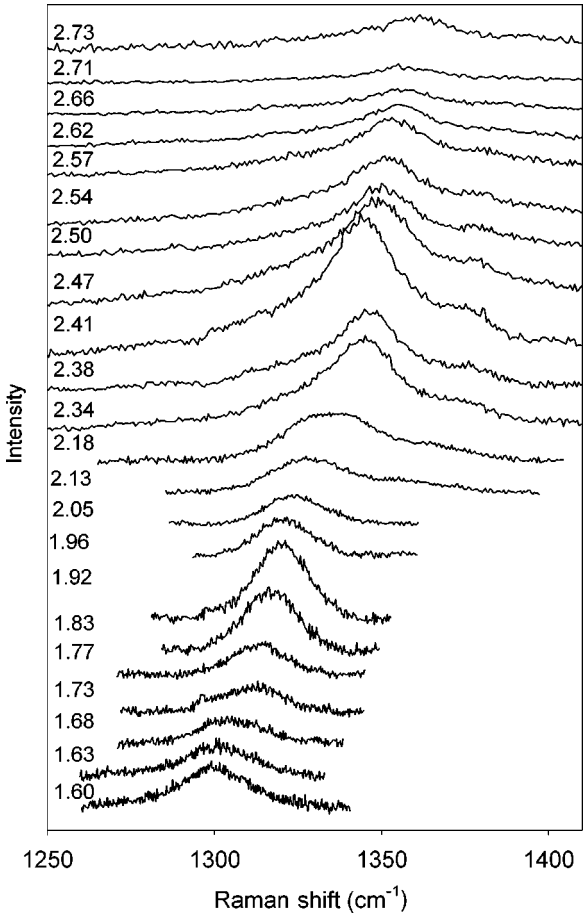

FIG. 7. D-band spectra measured by 22 different laser excitations for a sample of SWCNT's with Gaussian diameter distribution with a mean value of $d_0 = 1.32$ nm and a width of $\sigma = 0.14$ nm.

The least-squares fit for the linear part of the measured dispersion of the D band is

$$\omega_{max} = (1219 \pm 3) + (51.8 \pm 1.3) E_{laser}, \qquad (6)$$

where ω_{max} and E_{laser} are measured in cm^{-1} and eV, respectively.

The G' band also has an oscillation superimposed on a linear shift, similarly to the D band. The slope of the linear part for the G' band is about twice the slope of that of the D band. The G band has no dispersion.

The maximum intensity of the D band oscillates as well, showing two peaks at about 1.9 eV and 2.4 eV.

B. Comparison to theory

There are 114 different SWCNT's with diameters falling into the 3σ interval ($1.32 \pm 3 \times 0.14$ nm) corresponding to the measured sample. In principle, we had to carry out all necessary integrations for the 114 tubes to fit the measured D band of the sample. However, as we have shown in the preceding section, the position of the dominant peak in the D band of one single SWCNT is determined by the wave vec-

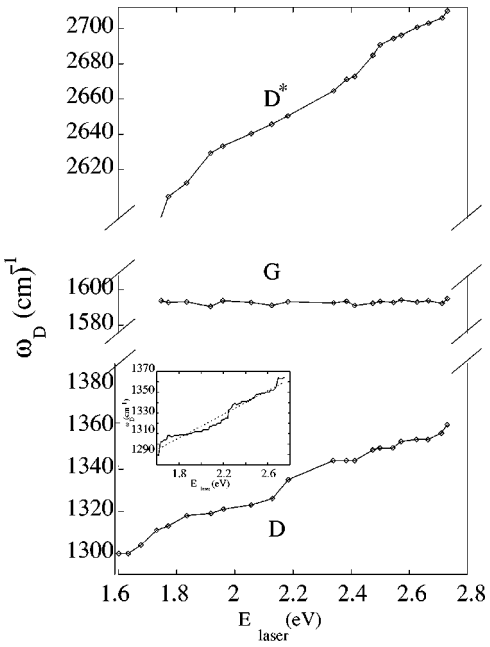

FIG. 8. Measured dispersion of the maximum position of the *D* band. For comparison, the behavior of the measured *G* and the *D** bands are also shown. The inset in the lower part shows the calculated maximum peak position vs laser excitation energy for a mixture of 114 different SWCNT's. The parameters of the Gaussian diameter distribution, which reproduced best the measured oscillation of the *D* band were: $d_0 = 1.32$ nm and $\sigma = 0.11$ nm.

tor(s) satisfying the ''triple resonance'' condition. It is a quick and easy task to find these wave vectors and the corresponding phonon frequencies for any given SWCNT. To obtain the resulting *D* band of the whole sample, the individual contributions for these vectors were summed up using the appropriate Gaussian weight factor of the diameter distribution. Due to the ''triple resonance'' condition, only tubes for which E_{laser} ($E_{las,1}$ or $E_{las,2}$) matches or nearly matches a vH singularity in the JDOS have a non-negligible contribution. This was taken into account by a square ''resonance window'' with a width of ± 0.1 eV centered around E_{laser} of both the incoming and outgoing laser light: only tubes for which a vH singularity fell into one of these ''resonance windows'' were considered for a given laser excitation energy. The smearing of the sharp ''stick'' frequency spectrum was carried out by a convolution with a Lorentzian curve with a half width of 10 cm^{-1}.

It turned out from the calculations that the oscillation in the maximum peak position of the resulting *D* band is very sensitive to the phonon-dispersion relation. Using formula (4) resulted in an oscillation with too large amplitude and in addition with too high frequency, obviously due to the too large anisotropy of the phonon dispersion. That was the reason for changing the phonon dispersion to the formula (5), where the amount of the anisotropy could be tuned, starting from zero. The anisotropy of $\delta = 0.06$ was found to result in a good fit of the measured oscillation. Note that an oscillation still remains even for the case of $\delta = 0$.) However, the details of this oscillation did not agree satisfactorily with those of the measured one.

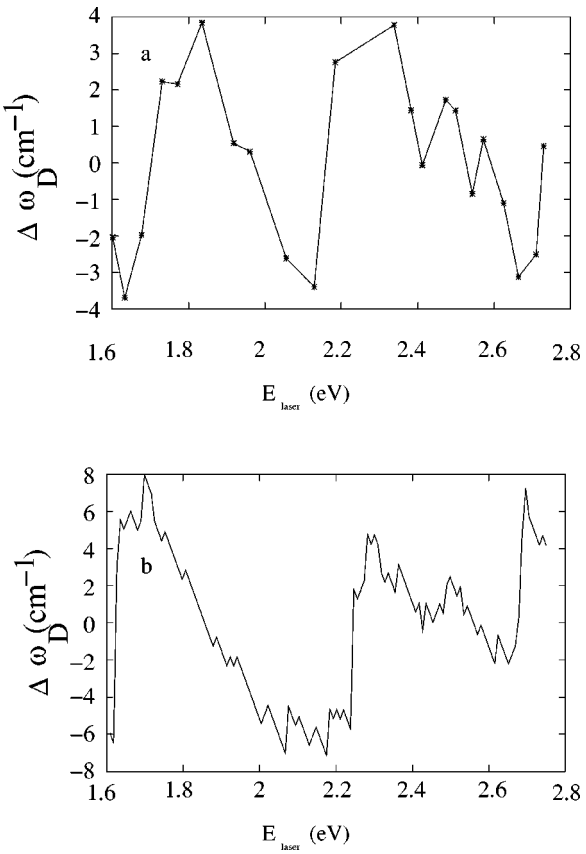

FIG. 9. Comparison between the measured (a) and calculated (b) oscillation in the maximum peak position. A linear progression was subtracted from the ω_D values.

To improve the fit the diameter distribution had to be changed as well. A small decrease in the width of the Gaussian distribution σ from 0.14 nm, as obtained from the RBM spectra, to 0.11 nm resulted in a significant improvement of the fit. Checking the RBM evaluation again we found that the average standard deviation of the calculated σ was estimated to be 0.03 nm.[5] Furthermore, comparing the σ values obtained from Raman RBM and from optics for the same samples, the deviation between them is in some cases even 0.04 nm.[4] We concluded from this that the analysis of the oscillation of the *D* band is more sensitive to the diameter distribution than the analysis of the oscillation of the RBM.

The inset in Fig. 8 shows the calculated anomalous dispersion of the *D* band. The least-squares fit for the linear part of the calculated dispersion is

$$\omega_{max} = (1203.4 \pm 1.1) + (56.9 \pm 2.3) E_{laser}, \qquad (7)$$

where ω_{max} and E_{laser} are measured in cm^{-1} and eV, respectively. This is in reasonable agreement with the measured values given by the formula (6).

Also, the measured oscillations can be reproduced well by our calculations as demonstrated in Fig. 9. The figure shows a comparison between the measured and calculated oscillations, where the linear progression was subtracted.

Finally, we discuss the qualitative reason for the anomalous dispersion (oscillation) of the *D* band of SWCNT's. The

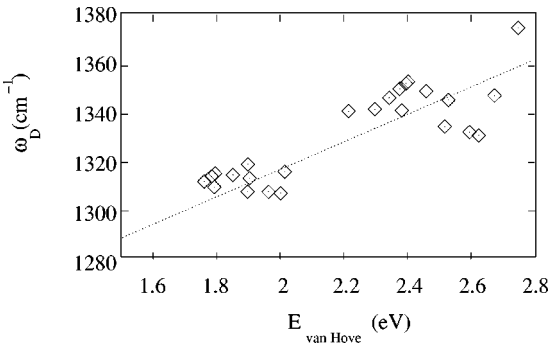

FIG. 10. Calculated *D*-band frequencies of the individual SWCNT's with diameters in the 1.32 ± 0.07 nm range as a function of the energies of the corresponding vH singularities.

origin of the behavior is the finite number of the different (n,m) chiralities in a typical sample together with the fact that the dependence of the *D*-band frequency on the position of a vH singularity in the *k* space is rather irregular. This is demonstrated in Fig. 10, where the *D*-band frequencies are plotted versus E_{vH} for only 18 nanotubes that have the largest weight factor, having diameters that fall into the very center part of the Gaussian distribution. We emphasize that nanotubes with the same diameter but with different chirality can have very different *D*-band frequencies; in this point the situation is different from the case of the RBM. The (n,m) chirality indices (not shown in the figure) scatter in a completely disordered manner. The discrete points in Fig. 10 already show the most important features of the oscillation. For this plot the model phonon dispersion (5) with a small anisotropy of $\delta = 0.06$ was used. A much larger anisotropy like in the formula (4) would result in a plot with much broader distribution of ω_D and as a consequence in an oscillation with much larger amplitude. On the other hand, for a very broad diameter distribution the oscillation would be averaged out and a linear shift would remain, similarly to the case of graphene. We mention that a linear shift in the position of the *D* band with changing the laser excitation energy can be obtained even for individual tubes if only the transitions along one discrete line (see e.g. Fig. 5) are taken into account. This behavior was already shown in Ref. 21 for a special class of nanotubes.

V. SUMMARY

The cross section of a higher-order Raman process in graphite exhibits a double resonance that results in a linear upshift of the position of the *D* band with increasing laser excitation energy. In this case two of the denominators (one for either the incoming or the outgoing light, and another one for an intermediate state of the system) become zero at the same time. SWCNT's have an anomalous dispersion relation as compared to graphite. We measured the dispersion of a sample consisting of different SWCNT's. We observed an oscillation superimposed on the linear upshift in the position of the *D* band. An oscillation in the intensity of the *D* band was observed as well. To interpret the experimental results we calculated the resonant Raman cross section carrying out explicit integrations of the formulas (1) and (2). We showed that the *D* band of a SWCNT is determined not only by double resonance alone. The intensity of the *D* band shows a sharp maximum when a vH singularity is matched by either the incoming or the outgoing light, as well— we use the abbreviation ''triple resonance'' for this effect. We have calculated the resulting *D* band of a sample consisting of 114 different SWCNT's with a Gaussian distribution for the diameters. Only the processes corresponding to the ''triple resonance'' were taken into account in this case, neglecting the contributions with much lower intensity. The calculation reproduced the measured anomalous dispersion very well. We have also shown that the analysis of the *D* band is more sensitive to the exact diameter distribution than the analysis of the RBM, therefore, it may serve as a useful method for the characterization of the SWCNT samples.

ACKNOWLEDGMENTS

This work was supported by the FKFP-0144/2000 and the OTKA T030435, T038014 grants in Hungary and by the Fonds zur Förderung der Wissenschaftlichen Forschung in Austria, Project P12924. Valuable discussions with A. Virosztek and J. Sólyom are gratefully acknowledged.

[1] For a comprehensive treatment of carbon nanotubes see, e.g., R. Saito, G. Dresselhaus, and M. S. Dresselhaus, *Physical Properties of Carbon Nanotubes* (Imperial College Press, London, 1999).

[2] See, e.g., *Electronic Properties of Molecular Nanostructures*, edited by H. Kuzmany *et al.*, AIP Conf. Proc. **591** (AIP, Melville, NY, 2001).

[3] M. Milnera, J. Kürti, M. Hulman, and H. Kuzmany, Phys. Rev. Lett. **84**, 1324 (2000).

[4] A. Grüneis, M. Hulman, Ch. Kramberger, T. Pichler, K. Peterlik, H. Kuzmany, H. Kataura, and Y. Achiba, in *Electronic Molecular Nanostructures*, Ref. 2, p. 319.

[5] M. Hulman, W. Plank, and H. Kuzmany, Phys. Rev. B **63**, 081406 (2001).

[6] A. Jorio, R. Saito, J.H. Hafner, C.M. Lieber, M. Hunter, T. McClure, G. Dresselhaus, and M.S. Dresselhaus, Phys. Rev. Lett. **86**, 1118 (2001).

[7] A. Grüneis, Diploma thesis, University of Vienna, 2001.

[8] M.A. Pimenta, E.B. Hanlon, A. Marucci, P. Corio, S.D.M. Brown, S.A. Empedocles, M.G. Bawendi, G. Dresselhaus, and M.S. Dresselhaus, Braz. J. Phys. **30**, 423 (2000).

[9] S.D.M. Brown, A. Jorio, M.S. Dresselhaus, and G. Dresselhaus, Phys. Rev. B **64**, 073403 (2001).

[10] F. Tuinstra and J.L. Koenig, J. Chem. Phys. **53**, 1126 (1970).

[11] R.P. Vidano, D.B. Fischbach, L.J. Willis, and T.M. Loehr, Solid State Commun. **39**, 341 (1981).

[12] I. Pócsik, M. Hundhausen, M. Koós, and L. Ley, J. Non-Cryst. Solids **227-230B**, 1083 (1998).

[13] M.J. Matthews, M.A. Pimenta, G. Dresselhaus, M.S. Dresselhaus, and M. Endo, Phys. Rev. B **59**, R6585 (1999).

[14] A.V. Baranov, A.N. Bekhterev, Y.S. Bobovich, and V.I. Petrov, Opt. Spectrosc. (USSR) **62**, 612 (1987).
[15] A.C. Ferrari and J. Robertson, Phys. Rev. B **64**, 075414 (2001).
[16] C. Castiglioni and C. Mapelli J. Chem. Phys. **114**, 963 (2001).
[17] G. Kresse, J. Furthmüller, and J. Hafner, Europhys. Lett. **32**, 729 (1995).
[18] D. Sanchez-Portal, E. Artacho, J.M. Soler, A. Rubio, and P. Ordejon, Phys. Rev. B **59**, 12 678 (1999).
[19] C. Thomsen and S. Reich, Phys. Rev. Lett. **85**, 5214 (2000).
[20] R.M. Martin and L.M. Falicov, in *Light Scattering in Solids*, edited by M. Cardona, Topics in Applied Physics Vol. 8 (Springer, Berlin, 1983).
[21] During the preparation of this paper our attention was drawn to another manuscript [J. Maultzsch, S. Reich, and C. Thomsen, Phys. Rev. B **64**, 121407 (2001)], where the idea of double resonance was adapted for SWCNT's. However, in this work the role of the vH singularities was completely neglected.
[22] An oscillation in the position of the *D* band of a bundle of SWCNT's was recently calculated [A.G. Souza Filho, A. Jorio, G. Dresselhaus, M.S. Dresselhaus, R. Saito, A.K. Swan, M.S. Ünlü, B.B. Goldberg, J.H. Hafner, C.M. Lieber, and M.A. Pimenta, Phys. Rev. B **65**, 035404 (2002)], emphasizing the role of the vH singularities, but neglecting the quantitative treatment of the double resonance.
[23] J. Renucci, R.N. Tyte, and M. Cardona, Phys. Rev. B **11**, 3885 (1975).